Aspects of Geneva photometry : part 2 : significance of multicolour photometry

Autor(en): **Cramer, Noël**

Objekttyp: **Article**

Zeitschrift: **Orion : Zeitschrift der Schweizerischen Astronomischen Gesellschaft**

Band (Jahr): **62 (2004)**

Heft 325

PDF erstellt am: **24.07.2024**

Persistenter Link: https://doi.org/10.5169/seals-898361

Nutzungsbedingungen

Die ETH-Bibliothek ist Anbieterin der digitalisierten Zeitschriften. Sie besitzt keine Urheberrechte an den Inhalten der Zeitschriften. Die Rechte liegen in der Regel bei den Herausgebern.
Die auf der Plattform e-periodica veröffentlichten Dokumente stehen für nicht-kommerzielle Zwecke in Lehre und Forschung sowie für die private Nutzung frei zur Verfügung. Einzelne Dateien oder Ausdrucke aus diesem Angebot können zusammen mit diesen Nutzungsbedingungen und den korrekten Herkunftsbezeichnungen weitergegeben werden.
Das Veröffentlichen von Bildern in Print- und Online-Publikationen ist nur mit vorheriger Genehmigung der Rechteinhaber erlaubt. Die systematische Speicherung von Teilen des elektronischen Angebots auf anderen Servern bedarf ebenfalls des schriftlichen Einverständnisses der Rechteinhaber.

Haftungsausschluss

Alle Angaben erfolgen ohne Gewähr für Vollständigkeit oder Richtigkeit. Es wird keine Haftung übernommen für Schäden durch die Verwendung von Informationen aus diesem Online-Angebot oder durch das Fehlen von Informationen. Dies gilt auch für Inhalte Dritter, die über dieses Angebot zugänglich sind.

Ein Dienst der *ETH-Bibliothek*
ETH Zürich, Rämistrasse 101, 8092 Zürich, Schweiz, www.library.ethz.ch

http://www.e-periodica.ch

Aspects of Geneva Photometry[1]

Part 2 - Significance of multicolour photometry

NOËL CRAMER

In this second part of the article, we discuss the significance of the multicolour photometric measurement. A multicolour system has properties similar to low resolution spectrophotometry by measuring the stellar spectral energy distribution and is, likewise, sensitive to temperature, luminosity and chemical composition effects. One of the more troublesome factors acting on such chromatic measurements is interstellar wavelength-dependent extinction by dust. A photometric system possessing a sufficient number of well distributed passbands can, nevertheless, largely compensate for interstellar reddening.

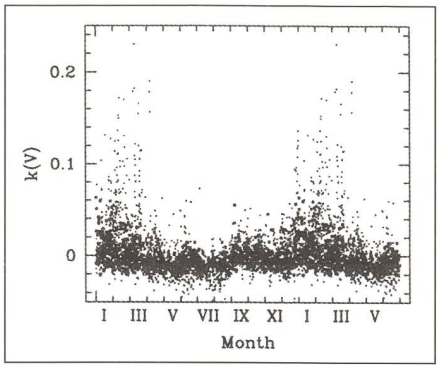

Fig 22: Cumulative annual variation of the extinction coefficient in V (mean wavelength 5488 Å) relative to its normal value of 0.130. The peaks are due to the increased aerosol content as the atmospheric inversion layer rises above the Observatory during the southern summer (BURKI et al, 1995).

3. The photometric measurement

The radiation flux in the wavelength interval (λ_1, λ_2) of a star seen by a ground-based observer is basically of the form:

$$F_{\lambda_1\lambda_2} = \int_{\lambda_1}^{\lambda_2} a^2 I(\lambda) T_i(\lambda,d) T_a(\lambda,d) T_t(\lambda) T_f(\lambda) r(\lambda) d\lambda$$

Where:

a Apparent diameter of star assumed to be spherical and to radiate isotropically.
$I(\lambda)$ Radiance of the star per unit wavelength interval.
$T_i(\lambda,d)$ Fraction of star's radiation transmitted by interstellar space in direction d.
$T_a(\lambda,d)$ Fraction of star's radiation transmitted by Earth's atmosphere in direction d.
$T_t(\lambda)$ Transmission of the telescope's optical system.
$T_f(\lambda)$ Transmission by filter f.
$r(\lambda)$ Response function of the detector.

The last two terms are assumed to depend only on λ but in reality they are also, to a lesser degree, temperature dependent. It is the reason why the photometers presented in Part 1 are thermostatically controlled.

The instrumental terms are habitually grouped as:

$$S(\lambda) = T_t(\lambda)\, T_f(\lambda)\, r(\lambda)$$

Which correspond to the passbands of Fig 1 (part 1).

The wavelength range of the integration above is ideally that where $S(\lambda) \neq 0$ only in the interval $[\lambda_1, \lambda_2]$ and where the other «terrestrial» term $T_a(\lambda,d) \neq 0$ over the same interval. Or, in other words, that the limits of the passbands are totally instrumentally-defined.

3.1. Atmospheric transmission $T_a(\lambda,d)$

The determination of the atmospheric transmission $T_a(\lambda,d)$ is a fundamental stage in the photometric reduction (see RUFENER, 1964). The subject is complex. It would necessitate a separate discussion and will not be examined here since we are interested in the astrophysical content of the photometric information. But it is noteworthy that the systematic measurement of that inevitable «nuisance» for the astronomer produces interesting data for the geophysicist and climatologist. Fig 21 shows the evolution of the extinction coefficient k(V) (expressed as extinction in magnitudes per unit air mass) in the V band measured by the Geneva telescope at the ESO La Silla Observatory, in Chile, over a period of 19 years (BURKI et al, 1995).

Conspicuous are the seasonal variations with their «summer spikes» (Fig 22) due to increased aerosol content when the atmospheric inversion layer occasionally rises above the Observatory (2400 m), and also the variations of the long term trend. The two abrupt increases of the latter were due to the eruptions of the El Chichon (Mexico, latitude +17°, March 23 and April 4, 1982) and the Pinatubo (Philippines, lat. +15°, June 12 to June 15, 1991) volcanoes. The volcanic contribution alone is shown in Fig 23 relative to the normal extinction coefficient in V. In fact, the El Chichon event took place just after the global atmospheric transparency had fully recovered from the effects of the explosive eruption of Mt. Agung in Bali on March 17, 1963.

The two volcanoes ejected some 8 and 20 megatons, respectively, of SO_2 into the stratosphere. That gas combines photochemically with atmospheric water vapour to form sulphuric acid H_2SO_4 droplets which are highly reflective and slowly decant through the atmosphere. The atmospheric extinction,

Fig 21: Variation of the visual extinction coefficient in magnitudes ($m_{0,V} = m_{z,V} - k(V)F_z$ where $m_{0,V}$ is the magnitude outside the atmosphere, $m_{z,V}$ the magnitude at zenith distance z and F_z the corresponding air mass) over a period of 19 years at La Silla (2400 m). Apart from the seasonal variations one notes the long term effects of the El Chichon and Pinatubo volcanic eruptions (BURKI et al, 1995)

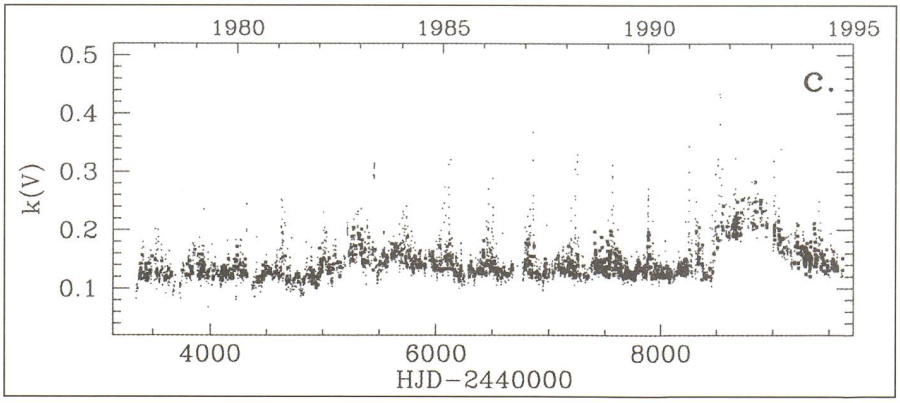

[1] Adapted from Archs Sci. Genève, Vol. 56, Fasc. 1, pp. 11-38, Juillet 2003. Based on data acquired at the La Silla (ESO, Chile), Jungfraujoch and Gornergrat (HFSJG International Foundation, Switzerland), and Haute-Provence (OHP, France) observatories.

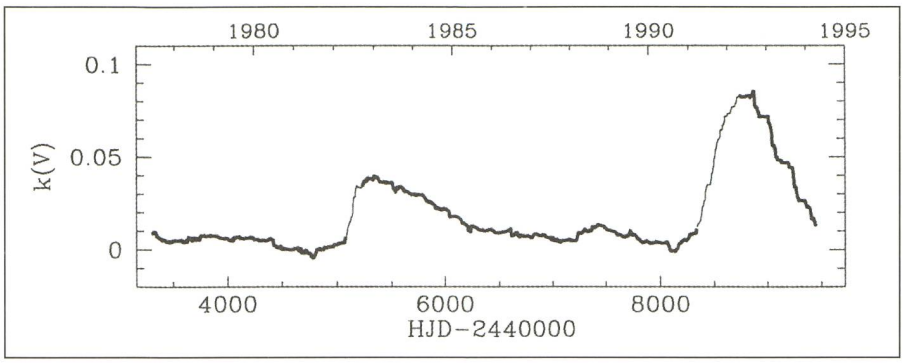

Fig 23: The volcanic contribution to the extinction coefficient in V relative to the normal value (BURKI et al, 1995).

normally about 9% vertically in the V band, reached 33% after the Pinatubo eruption and must have produced a potentially non negligible disruption of the global atmospheric thermal balance. A detailed analysis of these phenomena is given in BURKI et al, 1995.

3.2. After the reductions

Having gone through the reduction procedure, an elaborate and iterative process involving the conservation of the system, the photometric results are compiled in the Geneva Photometric Catalogue.

Photometric data are presented conventionally in «magnitudes» which are logarithmic expressions of flux ratios:

If the radiation fluxes of two stars in a *same* spectral range are in the ratio F_1/F_2, then their difference in magnitudes in that passband is:

$m_1 - m_2 = -2.5 \log (F_1/F_2)$ or, conversely $F_1/F_2 = 10^{-0.4(m_1 - m_2)}$

The scale of the *apparent visual magnitudes* m_v (magnitudes in passband V) is adjusted relatively to a conventional zero point (where $m_2 = 0$) in this manner and which roughly corresponds to the brightest stars visible in the night sky. Increasing magnitudes imply decreasing flux. The use of a decimal logarithmic scale is historical and is related to the physiology of eyesight, but it is also well suited to express the large range of fluxes observed for stars.

Likewise, if the flux measurements of a *given* star are made in two wavelength ranges (passbands) C_1 and C_2, then the flux ratio F_{C1}/F_{C2} transformed into the difference in magnitudes in these two ranges is the corresponding *colour index*:

$C_1 - C_2 = m_{C1} - m_{C2} = -2.5 \log (F_{C1}/F_{C2})$

To illustrate the general properties of colour indices, we may approximate the radiated spectral energy distribution of a star by the PLANCK function of a black body at different temperatures (Fig 24).

The energy distributions in Fig 24 can then be filtered (multiplied) by the photometric response functions of the passbands (for example the U, B, V bands, see Fig 1, Part 1) and we get the relative contributions of measured flux as seen in Fig 25.

To facilitate comparison, we have normalised the $B(T,\lambda)S(\lambda)$ functions at 4250 Å. We note that the true stellar energy distribution of the star Vega behaves differently from the ideal black body radiation due to its hydrogen absorption spectrum.

Note also that the *slope* of the source's energy distribution deforms the resulting filtered distribution and shifts the *effective mean wavelength* of the flux measurement in the ascending direction of the slope. This is true for all broad-band colour indices and can complicate the photometric analysis of stars by adding curvature to effects which would otherwise be linear for monochromatic indices. A complete discussion of bandwidth effects is made by GOLAY (1974).

Integrating over the curves in Fig 25 and building the respective surface (i.e. flux) ratios F_U/F_B and F_V/F_B and transforming into magnitudes as above, we get the (Geneva) colour indices of the classical U-B vs. V-B photometric diagram of Fig 26 where we have also plotted a sample of real stars into the same figure for comparison.

We see in Fig 26 that the photometric sequence of the real stars is basically a temperature sequence, as shown by the locus of the black body radiation in the colour index diagram. Incidentally, the slight curvature of the latter due to the band width effects invoked above is apparent in this figure. The departure of stars from the black body line is essentially due, at the higher temperatures, to the properties of hydrogen absorption in the stellar atmosphere (BALMER series and discontinuity due to the onset of continuous absorption short-ward of the BALMER jump), and at the lower temperatures to the apparition of molecular absorption affecting the visible spectrum.

Fig 24: The radiated energy distribution B(T,λ) of a black body at different temperatures on a logarithmic scale. The energy distribution of a real star (Vega) is shown in comparison roughly normalised to its «effective temperature» of 9500 K on the given scale.

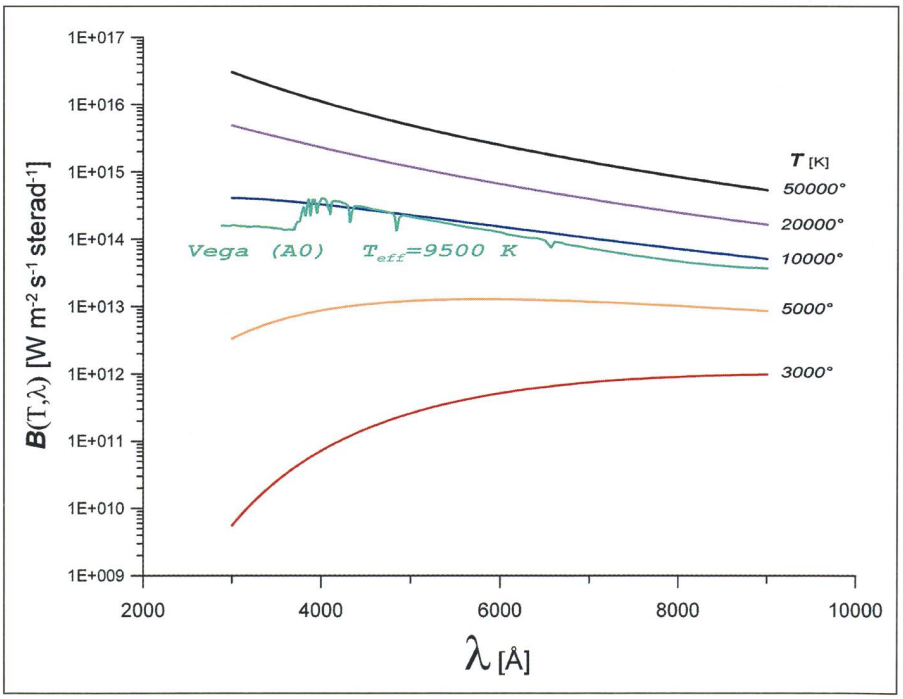

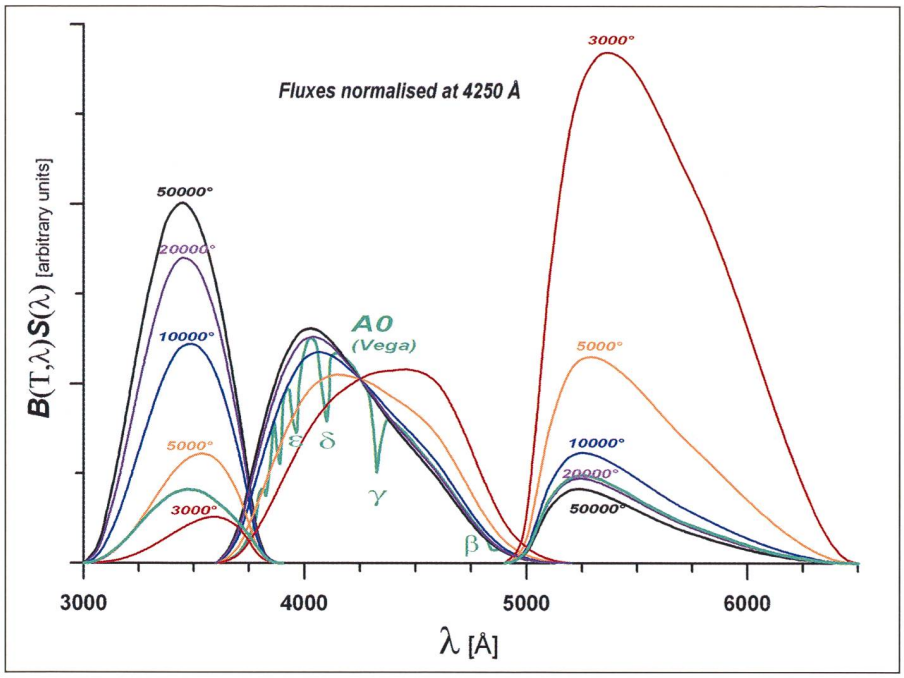

Fig 25: The «filtered» energy distributions B(T,λ)S(λ) of the black bodies of Fig 24 and of Vega, normalised at 4250 Å for the Geneva U, B and V passbands. We note the very different relative contributions according to temperature and the effect of the hydrogen absorption line spectrum for Vega. Note also the deformation of the filtered distributions with varying temperature.

Fig 26: The UBV diagram in the Geneva system with location of the MK spectral types. Only 1/4 of the measured stars are plotted for sake of clarity. The locus of black body radiation resulting from the temperatures considered in Figs 24 and 25 is shown. Vega, with its radiative energy distribution which is affected by the hydrogen absorption spectrum lies among the «real» stars, as it should.

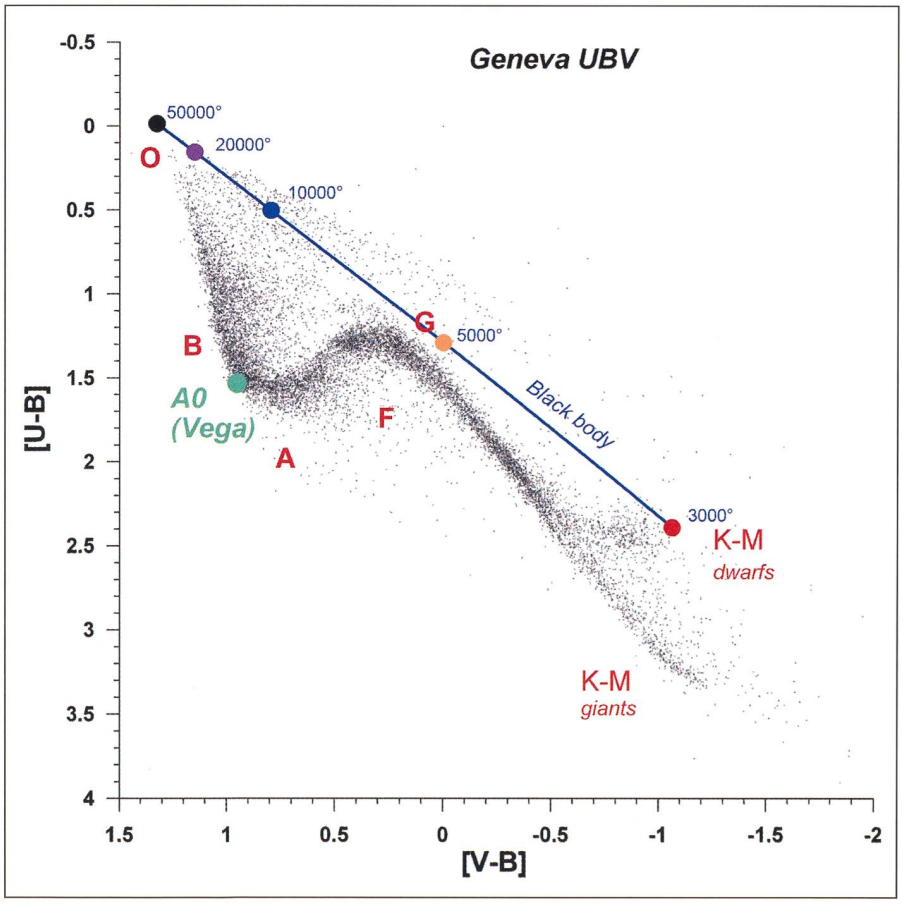

Therefore, it is customary to assign an *effective temperature* T_{eff} to real stars: If F is the *total* electromagnetic flux per surface unit (erg s^{-1} cm^{-2}) emitted *at its surface*, a star's T_{eff} is defined in terms of the Stefan-Boltzmann radiation law by $F = \sigma(T_{eff})^4$. The effective temperature is a basic parameter in stellar astrophysics.

One notes in Fig 27 (containing only stars having a MORGAN - KEENAN (MK) spectral classification) the large number of «reddened» O and B types which extend from the main sequence in the upper part of the diagram. That effect is extinction of starlight by interstellar dust. The curvature of the reddening line of the O stars is apparent for the most extreme values of extinction and is also due to band-width effects. The slight dispersion seen at more moderate reddening is due to small local variations of the wavelength dependence of the interstellar extinction law resulting from local properties of the dust grains.

Reddening, or interstellar extinction, is produced by wavelength-dependent attenuation of starlight by interstellar dust. The extinction is spectrally selective and the passbands of shorter wavelength are most affected (see Fig 29). Colour indices are shifted red-ward by a *«colour excess»* that is proportional to the optical depth of dust traversed.

The dust grains responsible for interstellar reddening are very small – some 0.25 μm down to several angstroms. They are believed to consist largely of carbon in the form of graphite, and oxides of magnesium, iron and silicon. The direct evidence for graphite is the strong ultraviolet absorption feature at 2175 Å (see fig 28) implying particles ≤ 0.015 μm, and for silicon oxides the presence of absorption bands in the infrared at 9.7 μm and 18 μm corresponding to amorphous silicates resembling olivine ($Mg_xFe_{2-x}SiO_4$). Another component related to carbon has recently been identified in the infrared with bands between 3.3 μm and 12 μm in emission. They are interpreted as being stretching modes of the C-C and C-H chemical bonds and imply the presence of polycyclic aromatic hydrocarbons (PAHs), which are planar molecules with organic benzene ring-like structures, on interstellar grains. Volatile compounds such as ices of water, methane, ammonia and other molecules composed of C, H, O, N can also be present in the cold conditions encountered in dark interstellar clouds, thus rendering the constitution of the dust particles sensitive to the intensity of the prevalent radiation field.

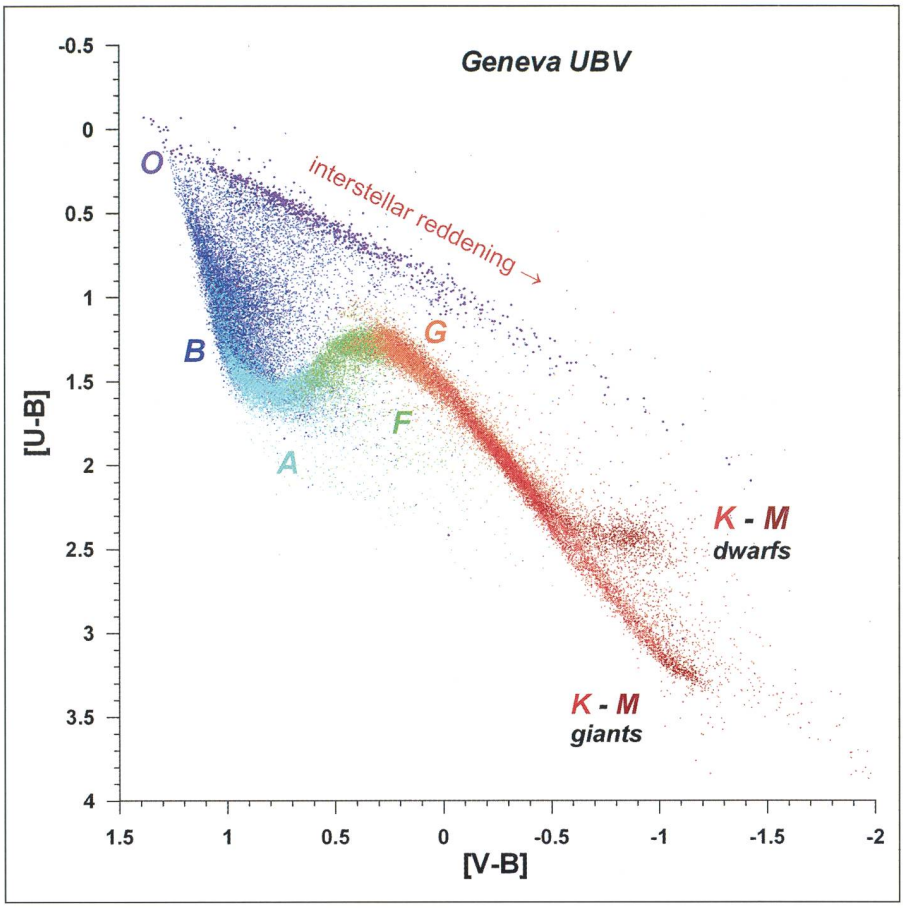

Fig 27: The Geneva UBV diagram showing the distribution of the MK (MORGAN – KEENAN) spectral types. Interstellar extinction (reddening) is most marked for the O-type stars which are very luminous, sparsely distributed and consequently the most distant in a sample limited in apparent magnitude. We note that, in this diagram, the more reddened B-type stars extend into the realm of the A, F and G-types. The few stars positioned below the O, B, A sequence are A and F-type supergiants.

The interstellar medium is complex and diverse, and is not yet fully understood. The detailed composition of dust grains is still subject to much debate. But, in the near infrared and visible parts of the spectrum, extinction by dust is largely governed by MIE scattering (extinction coefficient $Q_\lambda \approx a/\lambda$ where a = grain size) as may be seen in the quasi linear portion of fig 28. Extinction by dust has been the subject of very extensive modelling and we show as an example in fig 28 one (of several) computed by VAIDYA et al (2001) that gives a good account of the extinction curve in the visible. Models using different parameters reproduce the 2175 Å resonance better, but are less satisfactory at longer wavelengths. We also show the portion of the curve rendered in terms of colour excess ratios derived empirically in the Geneva system (CRAMER 1999). The overall agreement in the visible is very good.

Regarding the extinction seen in fig 27, we have seen that highly reddened B stars, through their colour excesses in U-B and V-B, can become indistinguishable in certain cases from cooler stars by merging with the type A, F or G sequence in this 3-colour diagram. Therefore, further information (i.e. a better sampling of the spectrum by more passbands) is needed for the proper analysis of systematically reddened stars.

4. Getting rid of $T_i(\lambda, d)$

4.1 Preliminary remarks concerning B stars

About 35% of the stars measured in the Geneva system can be loosely qualified in terms of the MK spectral classification as «B-type» (or, more precisely as O, B and first A-types). The hot, highly ionised, radiatively conducting atmospheres of these massive stars account for a relatively simple spectrum in the visible marked by the salient features of the BALMER jump and the hydrogen lines. Their spectral energy distribution, which is the dominant feature registered by multicolour photometry, is less affected by variations in chemical com-

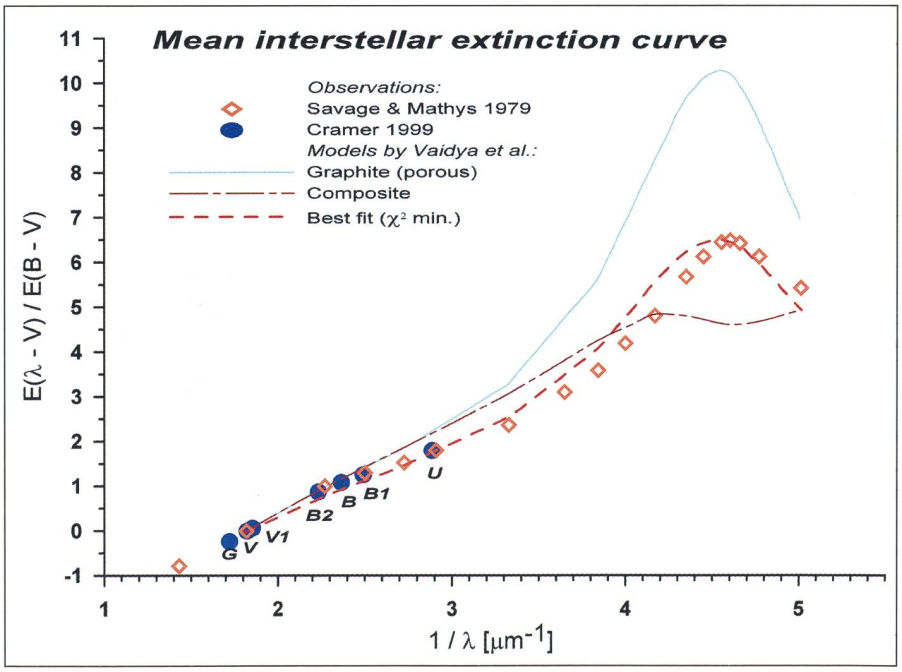

Fig 28: The mean interstellar extinction curve in terms of colour excess normalised to V (the vertical scale is sometimes given in terms of the absorption ratios A_λ/A_v). Observed values are by SAVAGE and MATHYS (1979), and by CRAMER (1999) for the spectral range covered by the Geneva system. The models are one of a set computed by VAIDYA et al (2001) for composites consisting of host silicate grains containing graphite inclusions and also associated with small «fluffy» porous graphite grains serving to reproduce the observed 2175 Å ($1/\lambda = 4.6\ \mu m^{-1}$) resonance of graphite absorption.

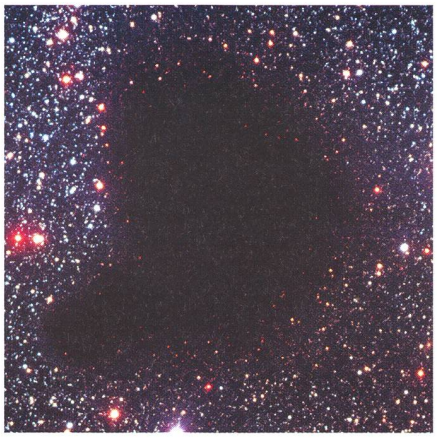

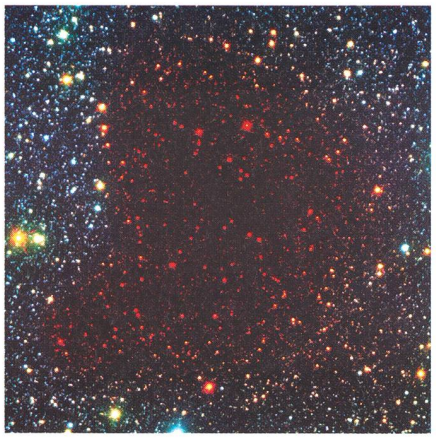

Fig 29: Interstellar reddening illustrated by the dark cloud BARNARD 68. All the stars in the field are in the background and one sees, left, their progressive «reddening» by dust extinction as the line of sight penetrates into the fringes of the cloud. Such dense "dark globules" are extreme examples of interstellar clouds consisting of gas and dust as they begin to contract and ultimately form new stars. BARNARD 68 is some 160 pc (500 light years) distant and only 0.2 pc in diameter. Observations using longer infrared wavelengths allow us to penetrate the central regions of the cloud as seen to the right, and show that it is in the very earliest phase of collapse with no evidence of star formation yet (Three-colour composites obtained with VLT ANTU + FORS1, European Southern Observatory).

position (elements heavier than Helium) than that of their cooler counterparts. Moreover, such rapidly evolving and consequently «contemporary» stars are not highly dispersed in initial chemical abundance (referred to as «metallicity» by astronomers) in our galactic neighbourhood since their population has not had time to be significantly subjected to mixing by galactic rotation. These factors reduce the colorimetric dispersion due to chemical composition and contribute to simplify the analysis in terms of basic quantities such as effective temperature and absolute luminosity.

B-type stars are, however, by their nature (short lifetime and lesser formation rate) much more sparsely distributed than cooler types, and their subsequently greater distances unavoidably link the study of their population by multicolour photometry to the effects of interstellar extinction by dust, as seen in Fig 27. Their analysis must therefore be done in a context that is corrected to the greatest possible extent for the colorimetric effects of extinction.

One way of rendering a multicolour photometric representation «immune» to interstellar reddening is to create one-dimensional *parameters* by projecting two-dimensional diagrams along their reddening line. Thus, we may for instance define a parameter Q_G in the Geneva system:

$Q_G = [U-B] + 0.654\,[V-B]$

Where 0.654 is the mean slope of the reddening line in the [U,B,V] diagram of Fig 27. We thus rectify that diagram in one of its dimensions and obtain, for example, the [Q_G, V, B] diagram of Fig 30. But, as in Fig 27, reddening also leads here to confusion by displacing B-type stars along the reddening-dependent [V-B] index into the sequence of cooler types.

However, for effective temperatures higher than about 10^4 K, and in contrast to cooler stars, the vectors of interstellar reddening in multi-dimensional parameter spaces incorporating additional passbands such as B1, B2, V1 and G stand well separated from those related to variations of the other major astrophysical quantities (effective temperature and surface gravity in the present context). This allows us to de-redden such stars with confidence and, conversely, to study the distribution of interstellar dust by measuring its extinction via the resulting «colour excesses» – just as the determination of the, at first sight, troublesome atmospheric absorption was put to use, above, to estimate its value and variation with time.

It is therefore profitable to go one step further by «projecting» selected colour index pairs along their reddening vectors, as above, and thereby defining reddening-free «colour spaces» generated by new sets of colour parameters.

4.2 The reddening-free representation adapted to B-type stars

The Geneva photometric catalogue lists the average values of the *normalised* reduced colours U, V, B1, B2, V1, G and the V-magnitude m_v of each object. These colours are in reality the colour indices [U-B], [V-B], [B1-B], [B2-B], [V1-B] and [G-B] normalised to B. Square brackets are used here by convention to distinguish the Geneva indices from those of other systems. The following relation allows the conversion of the indices listed in the catalogue into magnitudes:

$m_j = m_v - [V-B] + [j-B]$

Fig 30: The reddening-independent Q_G parameter of the Geneva system versus the [V-B] colour index. The [U, B, V] diagram of Fig 27 is thus rendered insensitive to interstellar extinction in one of its dimensions.

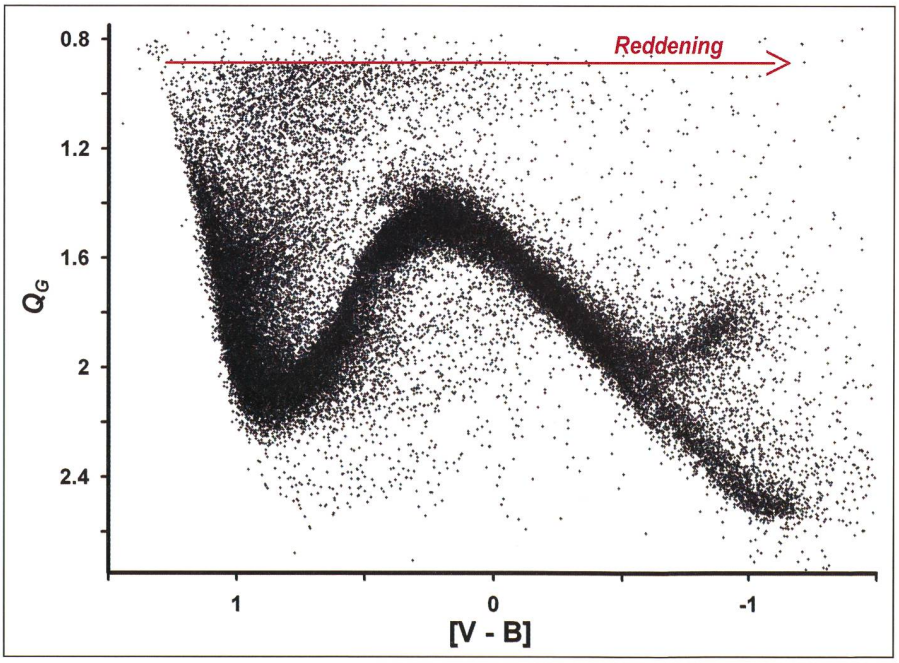

Where j is one of the 7 passbands.

The three traditional reddening-free parameters d, Δ and g of the Geneva system are each defined in the [U, B1, B2], [U, B2, G] and [B1, B2, G] diagrams, respectively, in a similar manner as Q_G shown above (see for example GOLAY, 1980):

d = [U-B1] – 1.430 [B1-B2]
Δ = [U-B2] – 0.832 [B2-G]
g = [B1-B2] – 1.357 [V1-G]

A transformation in the three-dimensional space generated by these parameters (CRAMER and MAEDER, 1979) leads to a new set of orthogonal parameters optimised for B-type stars and expressed here in terms of linear combinations of the normalised colours as follows:

X = 0.3797 +1.3764 U -1.2162 B1 -0.8498 B2 -0.1554 V1 +0.8449 G

Y = -0.8288 +0.3235 U -2.3228 B1 +2.3363 B2 +0.7495 V1 -1.0865 G

Z = -0.4572 +0.0255 U -0.1740 B1 +0.4696 B2 -1.1205 V1 +0.7994 G

The determination of these new parameters was initially done by translations and rotations involving successive approximations. A subsequent approach done by factorial analysis restricted to the B-type stars gave the same results within a margin better than 10^{-3} for the coefficients in the expressions above, and confirmed that no further modification was necessary.

The X parameter has properties which are similar to those of the U-B index by measuring the BALMER jump via U-B1, but benefits of a larger range of variation and has the important advantage of being reddening-free. It is the optimal temperature indicator for B stars in the Geneva system.

Y is much less sensitive to the BALMER discontinuity, but maximises the sensitivity to the width of the hydrogen lines via the B2-B1 index embedded in the relation. This makes it the best surface gravity indicator for B stars in the Geneva system. Surface gravity determines the local gas pressure, which affects the collisional broadening component of absorption lines. Finer lines mean fewer collisions, or less gas pressure, i.e. the extended atmosphere of a luminous and evolved giant or supergiant star.

Z is virtually independent of temperature and gravity effects. It optimises the detection of variations of gradient over the PASCHEN continuum in the range covered by the V band. Very weakly dispersed (σ ≡ 0.01 mag) for normal B stars, it detects «peculiarity» (Ap, Bp stars) and

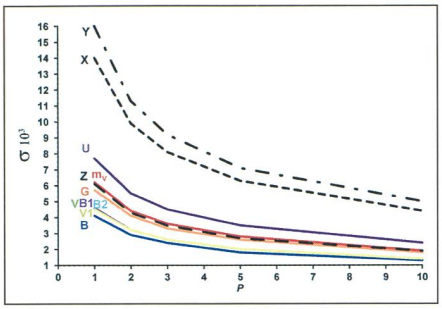

Fig 31: Probable internal errors of the colours, parameters and m_V in millimagnitudes as a function of the number of measurements used for the mean.

has been shown to be correlated, in restricted cases, with the surface magnetic field intensity via the 5200Å absorption feature that characterises such stars (CRAMER and MAEDER 1980).

The typical probable internal errors over the indices and parameters are given in Fig 31, where the weight P is synonymous with the number of good measurements contributing to the mean value in the catalogue.

The general features of this 3-dimensional representation are shown in the three projections into the (X,Y), (X,Z) and (Y,Z) planes of figures 32 to 34.

Noteworthy is the rectilinear sequence in fig 32 along the X axis starting at type O down to the first A-types where effective temperatures sink to about 10^4 K. The second important feature is the separation of evolved stars, culminating at the supergiant phase, from the non-evolved main sequence. The sequence of the B-type stars is rectilinear and much narrower in Z (Fig 33), which means that the Z parameter carries little astrophysical information for the «normal» B stars. The clean separation of the population of massive stars from those of lesser mass is put into better perspective by the Y, Z projection of fig 33, which thus confirms that the X and Y parameters are the most relevant of the three in regard to the intrinsic physical properties of the former.

Fig 32: The reddening-free representation of the Geneva X, Y, Z parameters with an indication of the locations of the MK spectral types. The X, Y diagram shown here demonstrates the optimisation for the early-type stars (types O, B and first A) which occupy an almost rectilinear sequence along the X direction with a separation of the giants and supergiants from the non-evolved sequence.

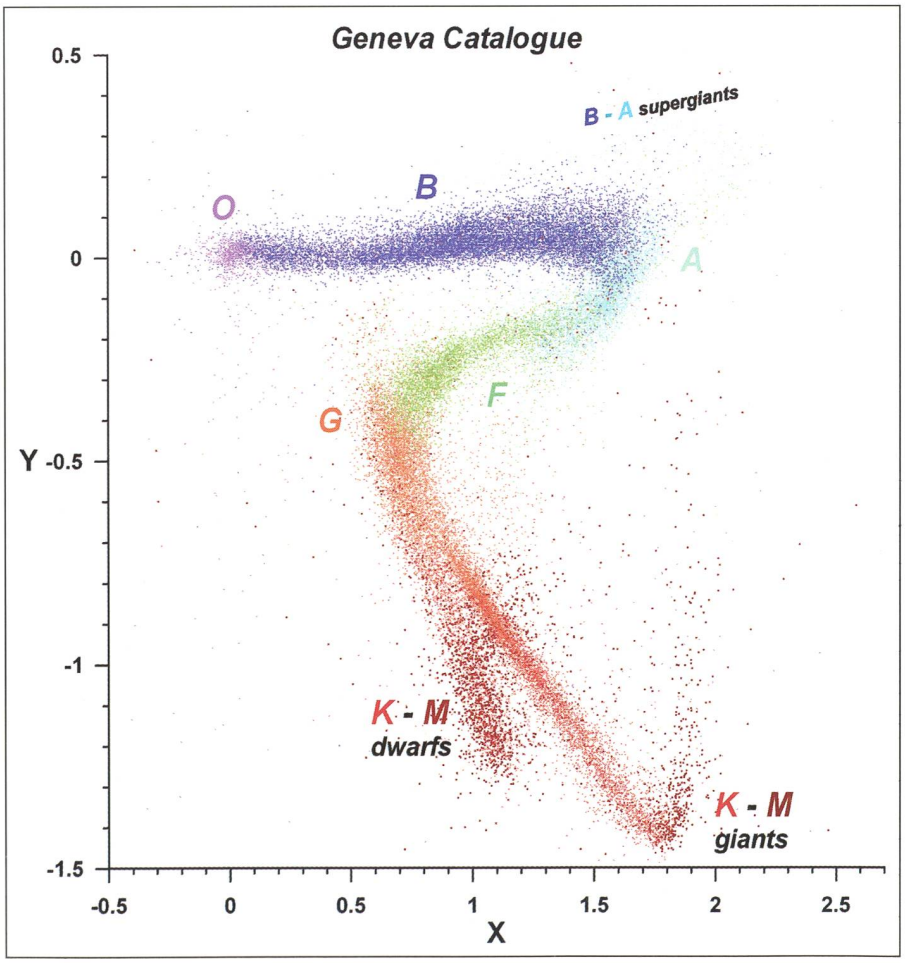

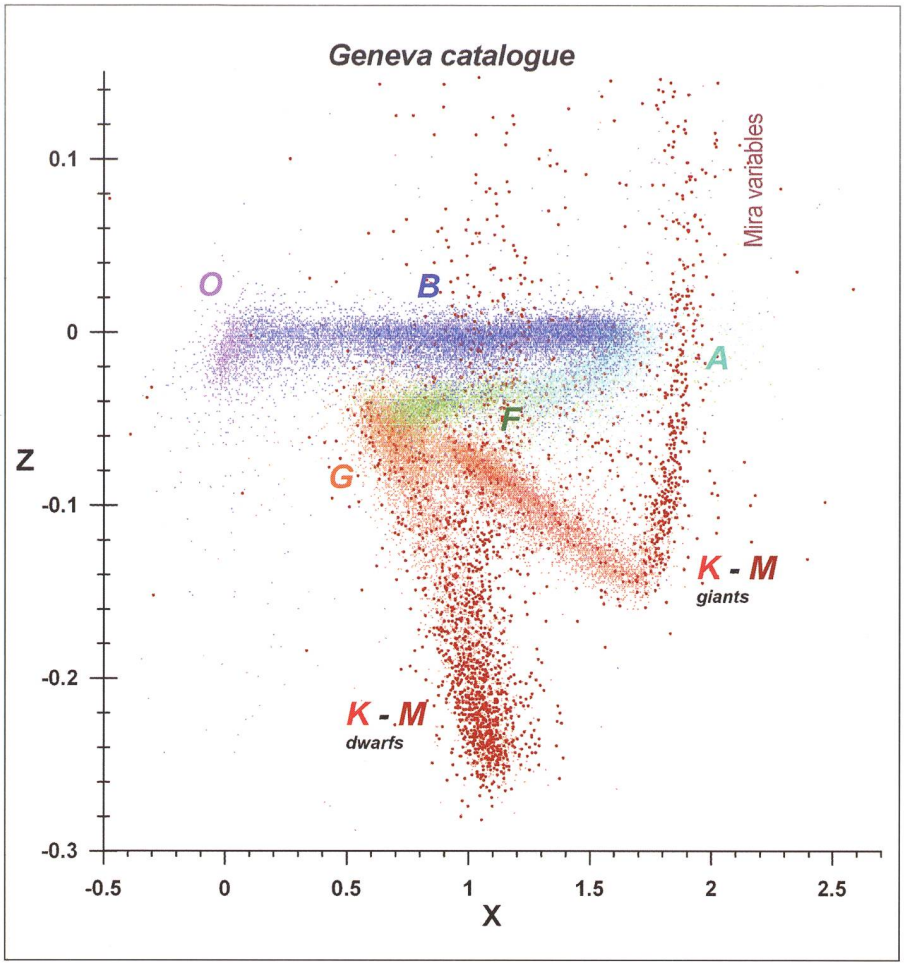

Fig 33: The X, Z diagram shows even better the rectilinear locus of the B-type stars. Note the extremely narrow sequence of the latter in the extended scale of the Z axis.

Bibliography 2:

BURKI, G., RUFENER, F., BURNET, M., RICHARD, C., BLECHA, A., BRATSCHI, P.: 1995, *The atmospheric extinction at the E.S.O. La Silla observatory*, A&AS 112, 383

CRAMER, N., MAEDER, A.:1979, *Luminosity and T_{eff} determinations for B-type stars*, A&A 78,305

CRAMER, N., MAEDER, A.:1980, *Relation between Surface Magnetic Field intensities and Geneva Photometry*, A&A 88, 135

CRAMER, N.: 1999, Calibrations *for B-type stars in the Geneva photometric system*, review article, New AR 43, 343

GOLAY, M.: 1974, *Introduction to Astronomical Photometry*, Reidel Publ. Co, Dordrecht

GOLAY, M.: 1980, *The Geneva Seven Colour photometric system*, review article in Vistas in Astronomy 24, part 2, A. Beer, K. Pounds, P. Beer eds., Pergamon Press, Oxford

RUFENER, F. : 1964, *Technique et réduction des mesures dans un nouveau système photométrique stellaire* (Thèse), Publ. Obs. Genève A, 66, 413

SAVAGE, B.D., MATHYS, J.S.: 1979, *Observed properties of interstellar dust*, review article, Ann. Rev. A&A, 17, 73

VAIDYA, D.B., GUPTA, R., DOBBIE, J.S., CHYLEK, P.: 2001, *Interstellar extinction by composite grains*, A&A 375, 584.

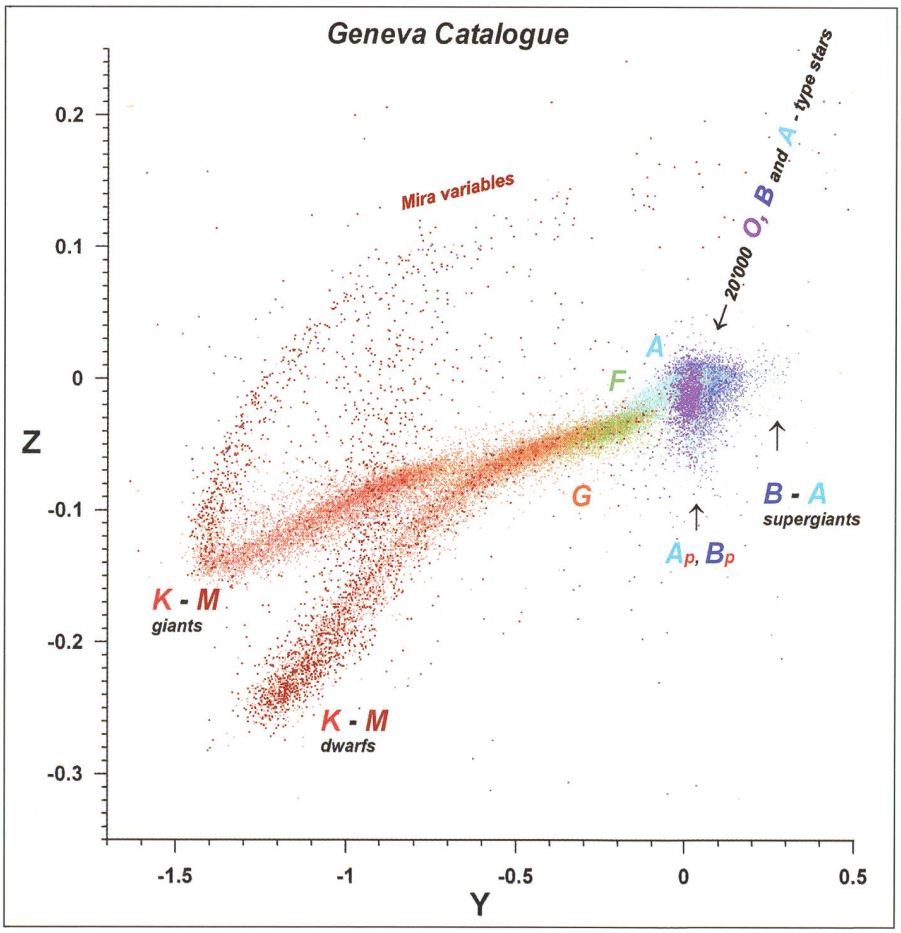

Fig 34: The Y, Z projection has the uncommon property of gathering about 20'000 O and B-type stars in the small clump to the right of the figure at Y=Z=0 thus demonstrating that two parameters (X and Y) suffice for their analysis. Those detaching themselves towards the extreme right are the early-type supergiants. Those descending and forming a sort of «beak» are the magnetic Ap and Bp stars. A closer examination of this 3-dimensional representation in the region occupied by the early-type (O to F) stars shows many similarities with the BARBIER – CHALONGE - DIVAN (BCD) classification mentioned in Part 1, Figs 2 and 3. This is to be expected since both representations are sensitive to the same features of the hydrogen spectrum in that region.

The obvious relationship between this three-parameter reddening-free representation and the basic physics that govern the radiative spectral energy distribution of stars suggests that the former can be applied in a quantitative manner. The next part of this article, related to the intrinsic properties of the stars will introduce the subject of photometric calibrations.

NOEL CRAMER
Observatoire de Genève
CH-1290 Sauverny